molecules

MDPI

Article

Iron Molybdate $Fe_2(MoO_4)_3$ Nanoparticles: Efficient Sorbent for Methylene Blue Dye Removal from Aqueous Solutions

Ahmed Mohmoud [1,2], Souad Rakass [3,*], Hicham Oudghiri Hassani [4], Fethi Kooli [5], Mostafa Abboudi [2] and Sami Ben Aoun [2]

1 Petroleum Technology, Operated Offshore Oil Field Development, Qatar Petroleum, Doha P.O. Box 3212, Qatar; caadil77@yahoo.co.uk
2 Department of Chemistry, Faculty of Science, Taibah University, Al-Madinah Al-Munawarah P.O. Box 30002, Saudi Arabia; abboudi14@hotmail.com (M.A.); sbenaoun@hotmail.com (S.B.A.)
3 Laboratory of Applied Organic Chemistry (LCOA), Chemistry Department, Faculty of Sciences and Techniques, Sidi Mohamed Ben Abdellah University, P.O. Box 2202, Imouzzer Road, 30000 Fez, Morocco
4 Engineering Laboratory of Organometallic, Molecular Materials and Environment (LIMOME), Faculty of Sciences, Chemistry Department, Sidi Mohamed Ben Abdellah University, P.O. Box 1796 (Atlas), 30000 Fez, Morocco; oudghiri_hassani_hicham@yahoo.com
5 Department of Chemistry, Faculty of Science, Islamic University of Madinah, Al-Madinah Al-Munawarah 42351, Saudi Arabia; fkooli@yahoo.com
* Correspondence: rakass_souad@yahoo.fr; Tel.: +212-6449950091

Academic Editor: Monika Wawrzkiewicz
Received: 29 September 2020; Accepted: 30 October 2020; Published: 3 November 2020

Abstract: The present study investigated iron molybdate ($Fe_2(MoO_4)_3$), synthesized via a simple method, as a nanosorbent for methylene blue (MB) dye removal from aqueous solutions. Investigations of the effects of several parameters like contact time, adsorbent dose, initial dye concentration, temperature and pH were carried out. The results showed that MB removal was affected, significantly, by adsorbent dose and pH. Interestingly, lower values of adsorbent dose resulted in the removal of higher amounts of MB. At the optimum pH, the removal efficiency of 99% was gained with an initial MB concentration of ≤60 ppm. The kinetic study specified an excellent correlation of the experimental results with the pseudo-second-order kinetics model. Thermodynamic studies proved a spontaneous, favorable and endothermic removal. The maximum amount of removal capacity of MB dye was 6173 mg/g, which was determined from the Langmuir model. The removal efficiency was shown to be retained after three cycles of reuse, as proven by thermal regeneration tests. The presence and adsorption of the dye onto the $Fe_2(MoO_4)_3$ nanoparticle surface, as well as the regeneration of the latter, was ascertained by scanning electron microscopy (SEM) and Fourier-transform infrared spectroscopy (FTIR). These findings are indicative that the investigated nanosorbent is an excellent candidate for the removal of MB in wastewater.

Keywords: nanosorbent; $Fe_2(MoO_4)_3$; removal; methylene blue; regeneration

1. Introduction

The textile and dyeing industries are major problem sources of water pollution [1,2]. Dye effluent released into clean water causes a variety of health hazards in marine organisms, freshwater sources and humans [2]. Thus, dyes are considered to be highly toxic and carcinogenic, and their removal is of great interest.

Therefore, several methods have been developed and employed for the removal and/or degradation of hazardous organic dyes from contaminated wastewater, such as photodegradation, extraction, adsorption, membrane separation, coagulation, flocculation, chemical oxidation, ion exchange and biological treatment [3–9]. Among all the techniques, adsorption by natural and synthetic adsorbents has been widely used because of its simplicity and efficiency for toxic dye removal in wastewater [10–15].

Several natural adsorbents are effective in removing dyes from aqueous effluents [10,11,16,17], of which activated carbon is the most commonly used, mainly due to its superior adsorption efficiency [18,19]. Nevertheless, commercially available activated carbon is very expensive [20].

There is therefore a great need to develop efficient adsorbents showing superior performance in their ability to remove pollutants and having suitable properties, such as ease of separation from the solution, regeneration and efficiency, even after several cycles of use, in order to enable the recovery of valuable compounds.

In recent decades, metal oxides as potential materials with different capabilities have been studied [21]. The family of metal molybdates is one of the most promising examples of the mixed metal oxides, which have been extensively studied in recent years [22–25].

Metal molybdate compounds with the formula $MMoO_4$ or $M_2(MoO_4)_3$ are important inorganic materials that have attracted great research interest, because they have important industrial applications. These include photocatalytic materials, humidity sensors, scintillator materials, photoluminescent compounds and optical fibers [26,27]; microwave applications and electrochemical and magnetic properties are also key features of these compounds. Metal molybdate compounds synthesized in the nanoscale were also used for environmental applications such as the removal of dyes from water by adsorption [23,28], oxidation of methylene blue dye [29] and photocatalytic oxidation of dyes [30].

Among all molybdenum-containing mixed oxides, the most studied is perhaps iron molybdate $Fe_2(MoO_4)_3$. It has garnered an exponentially increasing degree of interest, it has been synthesized at the nanoscale by different methods and it has been involved in many environmental and industrial applications [31]. In fact, iron molybdate has important applications in solid oxide fuel cells, sodium and lithium ion batteries, catalysis and sensors [32], propylene oxide production via the oxidation of propylene [33,34], methanol oxidation to formaldehyde [35] and photo-combined heterogeneous activation of persulfate for the removal of micropollutants [36]. In addition, the coprecipitation preparation of $Fe_2(MoO_4)_3$ nanopowder was applied for the photocatalytic degradation of rhodamine B with an efficiency of ~97% [37].

In the present work, iron molybdate nanoparticles prepared at a rather low temperature via a relatively cost-effective and very simple procedure, as previously described in the literature [22], were investigated as an adsorbent for MB dye removal. The effects of different parameters such as solution pH, temperature, contact time, adsorbent dosage and initial dye concentration on the removal of MB by the synthesized $Fe_2(MoO_4)_3$ nanosorbents were studied. In addition, the adsorption isotherms and kinetics were evaluated. Furthermore, the removal efficiency after regeneration of the used nanosorbent by calcination at high temperature was evaluated.

2. Results and Discussion

2.1. MB Removal

2.1.1. pH Effect

An essential parameter in terms of controlling the dye removal is pH [38]. While it does not modify the adsorbent site separation, it nevertheless changes the chemistry and the structure of the dye [39]. Therefore, the effect of pH on MB removal using iron molybdate $Fe_2(MoO_4)_3$ nanosorbent was investigated by varying its values between 3 and 11 at room temperature (i.e., 20 °C) with an initial concentration of 80 ppm. As shown in Figure 1, there is a pronounced effect of pH on MB removal. For instance, an increasing removal percentage from 69% to 88% was observed with increasing pH values from 3 to 11. The same trend was also observed for the dye removal amount per adsorbent

unit mass at equilibrium (q_e), which increased from 110 to 137 mg/g. There was a strong electrostatic interaction of the charges between the MB dyes and the $Fe_2(MoO_4)_3$ adsorbent, and this was shown by increasing the pH values, which resulted in a higher percentage obtained. In fact, the hydroxyl group (OH^-) in the solution at pH 11 favors the positive charge of the MB, which has a pKa equal to 3.8 [40]. However, at acidic values, the lower removal efficiency could be linked to the excess of proton ions in the solution competing with the basic dye cations on the removal sites of $Fe_2(MoO_4)_3$. Similar findings were reported by Kooli et al. [41] in a study of waste bricks applied as a promising removal agent for basic blue 41 from aqueous solutions. Thus, the best value for MB removal using $Fe_2(MoO_4)_3$ nanosorbent was shown at pH 11.

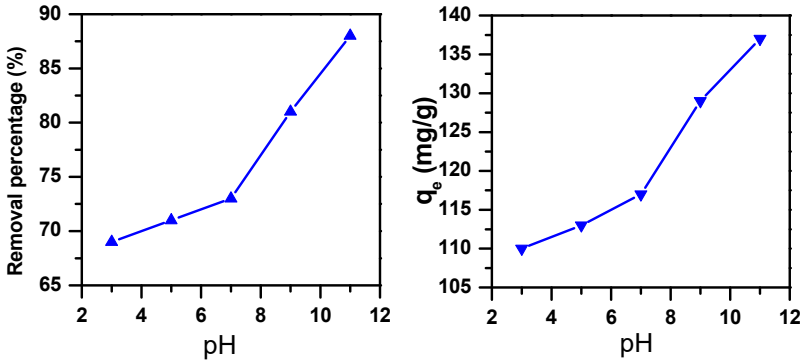

Figure 1. Removal efficiency of $Fe_2(MoO_4)_3$ in an 80-ppm methylene blue (MB) solution as a function of pH (m_{ads} = 0.05 g, T = 20 °C, t = 30 min).

2.1.2. Adsorbent Dose Effect

The adsorbent dose is regarded as one of the important parameters in the adsorption processes [42]. MB dye removal using $Fe_2(MoO_4)_3$, with an initial dye concentration of 70 ppm, was explored by varying the dose of the adsorbent between 0.001 and 0.05 g/L. As can be depicted from Figure 2, the percentage (%) of removed MB increased, and its concentration (mg/g) decreased when the adsorbent dose increased from 0.001 to 0.05 g/L. This was an expected tendency, since the active sites of the adsorbent's surface area increase with the increasing adsorbent dose, which therefore leads to an increasing amount of removed MB [43].

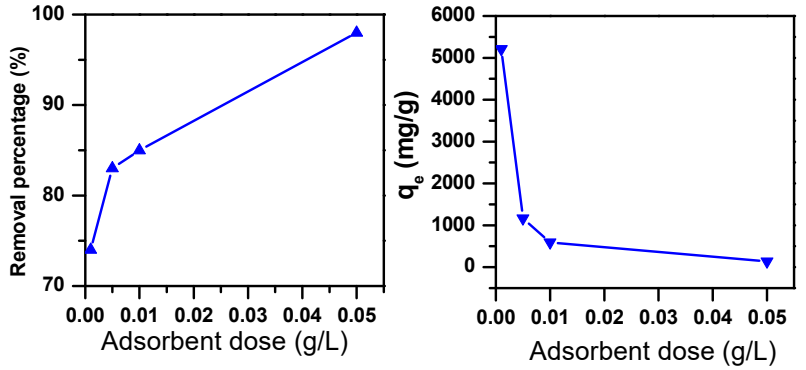

Figure 2. Removal efficiency of $Fe_2(MoO_4)_3$ in a 70-ppm MB solution as a function of the adsorbent dose (t = 30 min, T = 20 °C).

2.1.3. Initial Dye Concentration and Contact Time Effect

Removal studies, in light of the effect of initial MB dye concentration and contact time, were conducted at pH 11, and the results are shown in Figure 3. A percentage of 95% removal was achieved within 30 min for both C_i of 50 and 60 ppm, which increased to 99% after a 120-min

contact time. As for a C_i value of 65 ppm, the removal percentage maximum (92%) was reached with a contact time of 120 min. However, removal maxima of 88% and 76% were obtained with C_i values of 70 and 80 ppm, respectively, after a 120-min contact time. Thus, the removal capacity increased notably from 4999 mg/g to 6179 mg/g with increasing initial concentrations of dye from 50 to 80 ppm. Such a trend could be attributed to the initially abundant empty sites onto the $Fe_2(MoO_4)_3$ surface, which, as a consequence of the sorption process, gradually decreased by filling up these sites with increasing contact times [44].

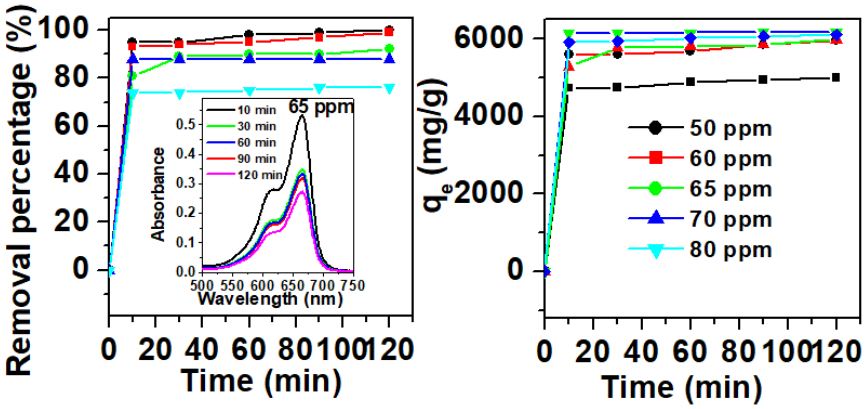

Figure 3. Removal efficiency of $Fe_2(MoO_4)_3$ for methylene blue (MB) as a function of initial dye concentration and contact time ($m_{adsorbent}$ = 0.001 g, T = 20 °C). Inset: UV spectra of MB solutions (65 ppm) after contact with $Fe_2(MoO_4)_3$ as a function of time.

2.1.4. Temperature Effect

Temperature is another parameter of prime importance that has a great impact on dye removal [45]. The process of removing the MB dye was investigated from 20 to 70 °C, as can be seen in Figure 4. The effect of temperature studies showed that the percentage removal increased from 76% to 99% at an initial dye concentration of 80 ppm, with an increased removal capacity from 6109 mg/g to 7999 mg/g. In fact, the removal motion of the adsorbent sites improved with increasing temperature, which, in turn, caused the motion of the dye molecules to increase [46].

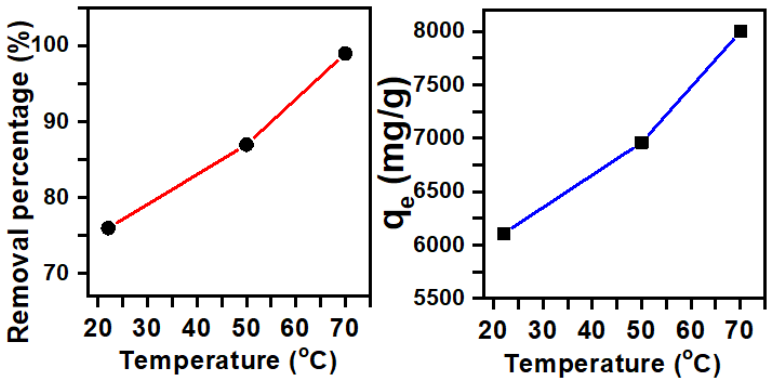

Figure 4. The removal efficiency of $Fe_2(MoO_4)_3$ in a 80-ppm MB solution as a function of temperature (t = 30 min, pH = 11).

Thermodynamic factors are important parameters in the adsorption processes [47]. The probability and the adsorption mechanism are predictable in the light of thermodynamic parameters [47]. These can be evaluated by means of the following equations:

$$\Delta G^o = -RTLnK_d \quad (1)$$

$$K_d = \frac{C_a}{C_e} \quad (2)$$

$$LnK_d = \frac{\Delta S^o}{R} - \frac{\Delta H^o}{RT} \quad (3)$$

where K_d is the distribution constant, T is the absolute temperature (K), R is the gas constant ($J.mol^{-1}.K^{-1}$), $\Delta G°$ is the free energy, C_a is the amount of dye adsorbed at equilibrium, C_e is the equilibrium concentration (mol/L) and $\Delta H°$ and $\Delta S°$ are the standard enthalpy and standard entropy, respectively. The values of $\Delta S°$ and $\Delta H°$ were determined from the intercept and slope of the plot ln K_d versus 1/T (Figure 5), and $\Delta G°$ values were calculated from Equation (1). All data are shown in Table 1.

The negative sign of $\Delta G°$ indicated a favorable and spontaneous adsorption. The removal of MB dye, as indicated by the positive value of $\Delta H°$ (83.79 $KJ.mol^{-1}$), was proven to occur via a physisorption process [48]. The positive values of $\Delta S°$ were proof of the increased randomness and disorder at the solid–solution interface of $Fe_2(MoO_4)_3$ and MB. The adsorbate molecules caused the adsorbed water molecules to move, and consequently, an additional translational energy was gained, resulting in a random system taking place [49].

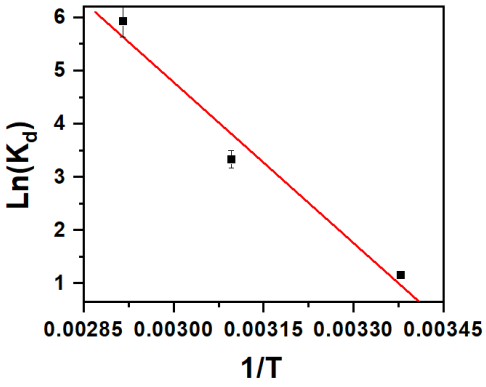

Figure 5. Van 't Hoff plot showing the effect of temperature on MB removal by $Fe_2(MoO_4)_3$.

Table 1. Methylene blue (MB) removal by $Fe_2(MoO_4)_3$ thermodynamic parameters.

Adsorbent	Adsorbate	ΔH° (KJ·mol^{-1})	ΔS° (KJ·mol^{-1}·K)	ΔG° (KJ·mol^{-1})		
				296K	323K	343K
$Fe_2(MoO_4)_3$	MB	83.79	0.291	−2.904	−8.934	−16.402

2.2. Kinetic Study

A kinetic test for the removal of MB was investigated in order to provide an indication regarding the adsorption system [38].

The kinetics of MB dye elimination using $Fe_2(MoO_4)_3$ nanosorbent were evaluated using intraparticle diffusion and pseudo-first-order and pseudo-second-order kinetic models. The equations of the considered models are given in Table 2.

The three model parameters, namely intraparticle diffusion, pseudo-first-order and pseudo-second-order, are arranged in Table 3 and shown in Figures 6–8, respectively. These models varied in the values of correlation coefficients (R^2) of the linear regressions. These values were estimated as follows: 0.748 to 0.993 for intraparticle diffusion, 0.752 to 0.993 for pseudo-first-order model and 0.999 to 1.000 for pseudo-second-order model for the studied concentrations. Since the R^2 value was equal to or near 1 for the pseudo-second-order model, the latter fit very well to the experimental data.

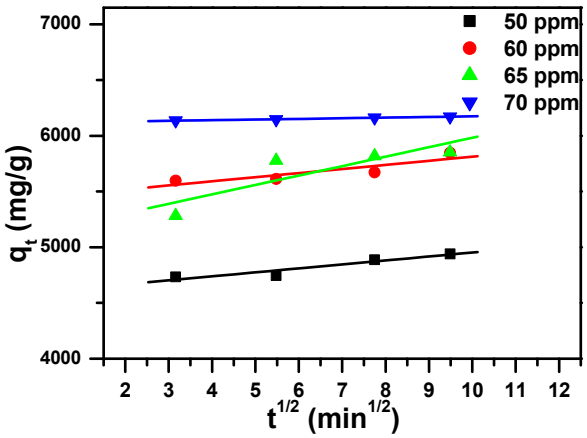

Figure 6. Intraparticle diffusion model plot showing the effect of contact time and initial dye concentration of MB removal by $Fe_2(MoO_4)_3$.

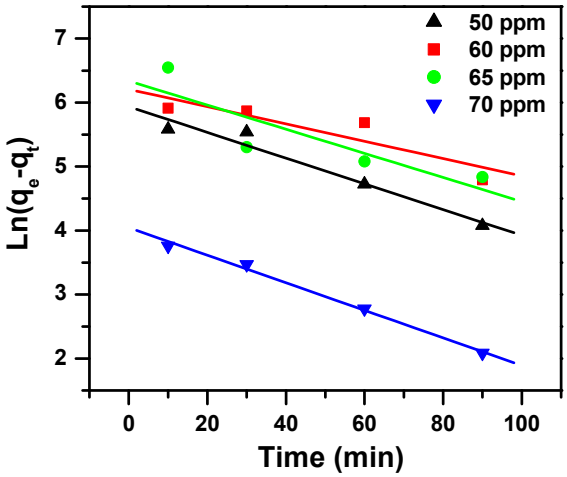

Figure 7. Pseudo-first-order model plot showing the effect of contact time and initial dye concentration on MB removal using $Fe_2(MoO_4)_3$.

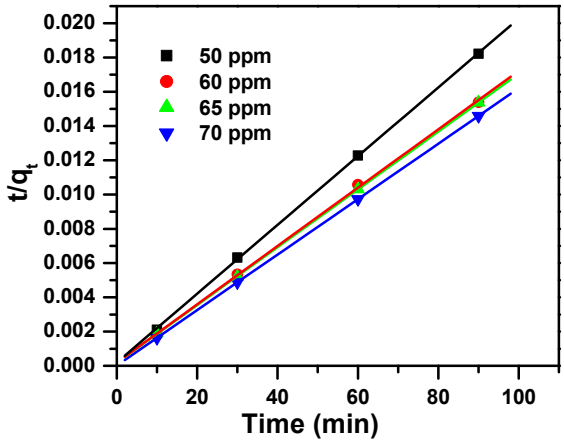

Figure 8. Pseudo-second-order model plot showing the effect of contact time and initial dye concentration of MB removal by $Fe_2(MoO_4)_3$.

Table 2. Kinetic model equations.

Model	Equation	Parameters
Pseudo-first-order (PFD) [50]	$\ln(q_e - q_t) = \ln\ q_e + K_1 t$ (4)	q_t: the removal capacity at time t (mg/g) q_e: the removal capacity at equilibrium (mg/g) K_1: the rate constant of pseudo-first-order adsorption (1/min)
Pseudo-second-order (PSD) [50]	$\frac{t}{q_t} = \frac{1}{K_2 q_e^2} + \frac{t}{q_e}$ (5)	q_t: the removal capacity at time t (mg/g) q_e: the removal capacity at equilibrium (mg/g) K_2: the pseudo-second-order rate constant (g. mg^{-1}.min^{-1})
Intraparticle diffusion (IPD) [51]	$q_t = K_I t^{0.5} + I$ (6)	I (mg/g) and K_I (mg/(g.$min^{0.5}$)) are the intraparticle diffusion constants q_t: the removal capacity (mg/g) at time t t: the contact time (min)

Table 3. MB removal by $Fe_2(MoO_4)_3$ kinetic parameters.

Dye (C_i mg/L)	Pseudo-First-Order				Pseudo-Second-Order			Intraparticle Diffusion Model		
	q_{exp} (mg/g)	q_e (mg/g)	k_1 (1/min)	R_1^2	q_e (mg/g)	k_2 (g/mg min)	R_2^2	I (mg/g)	k_i (mg/g $min^{0.5}$)	R_3^2
50	4999	378	0.020	0.956	4981	0.00021	1.000	4596	36	0.904
60	5967	496	0.014	0.814	5871	0.00016	0.999	5444	37	0.782
65	5979	565	0.019	0.752	5922	0.00016	1.000	5135	85	0.748
70	6179	57	0.021	0.993	6176	0.00154	1.000	6117	6	0.993

2.3. Adsorption Isotherms

It is essential to examine adsorption isotherms because of the information they provide when planning to use the adsorption method [50]. In the present work, we studied the four major adsorption models, namely Freundlich, Langmuir, Dubinin-Radushkevich and Temkin. These are governed by the equations presented in Table 4.

The Dubinin-Radushkevich, Temkin, Freundlich and Langmuir models were studied and attempted to fit the experimental data. The model parameters and the regression correlation coefficients (R^2) are given in Table 5, as extracted from Figure 9. The highest value for R^2 (0.999) was obtained from the Langmuir model, while the fittings of the Freundlich and Temkin models showed the lowest values of R^2 (0.866 and 0.870, respectively), whereas an intermediary value was achieved for the D-R model (R^2 = 0.971). Accordingly, the Langmuir isotherm had the best fit with the experimental results, suggesting that the dye removal proceeded via the formation of an MB monolayer onto the $Fe_2(MoO_4)_3$ adsorbent surface, with a high adsorption capacity of 6173 mg/g, leading to a homogenous surface. On the other hand, the separation factor R_L, ranging from 0.0024 to 0.0038, indicated a favorable dye removal by $Fe_2(MoO_4)_3$. Therefore, the investigated nanosorbent had excellent removal efficiency when compared to other materials (Table 6).

Table 4. Adsorption isotherm models for MB dye removal using $Fe_2(MoO_4)_3$.

Model	Equation	Parameters
Freundlich [52]	$\ln\ q_e = \ln\ q_F + \frac{1}{n}\ln\ C_e$ (7)	q_F: Freundlich constant ($mg^{(1-1/n)}L^{1/n}g^{-1}$) n: heterogeneity factor (g/L) q_e: amount of MB dye adsorbed by α-$Fe_2(MoO_4)_3$ at equilibrium (mg/g) C_e: MB concentration at equilibrium (ppm)
Langmuir [52]	$\frac{C_e}{q_e} = \frac{1}{q_m K_L} + \frac{C_e}{q_m}$ (8)	q_e: amount of MB dye adsorbed by α-$Fe_2(MoO_4)_3$ at equilibrium (mg/g) C_e: MB concentration at equilibrium (ppm) q_m: maximum amount of MB dye removed by $Fe_2(MoO_4)_3$ (mg/g) K_L: Langmuir adsorption constant (L/mg)
	$R_L = \frac{1}{1+K_L C_i}$ (9)	C_i: initial concentration of MB K_L: Langmuir constant R_L: values specify that the removal of MB dye could be linear (R_L = 1), irreversible (R_L = 0), favorable (0 < R_L < 1) or unfavorable (R_L > 1)

Table 4. *Cont.*

Model	Equation	Parameters
Dubinin-Radushkevich (D-R) [53]	$\ln q_e = \ln q_m - K\varepsilon^2$ (10) $\varepsilon = RT \ln\left(1 + \frac{1}{C_e}\right)$ (11)	K: sorption energy constant (mol^2/kJ^2) ε: Polanyi potential T: temperature (K) R: universal gas constant (8.314 $J.mol^{-1}$ K^{-1}) q_m: theoretical saturation capacity C_e: MB concentration at equilibrium (ppm)
Temkin [54]	$q_e = B_T \ln A_T + B_T \ln C_e$ (12)	b_T: Temkin constant related to heat of sorption (J/mol), $B_T = R_T/b_T$ R: gas constant (8.314 J/mol K) A_T: Temkin isotherm constant (L/g) T: absolute temperature (K)

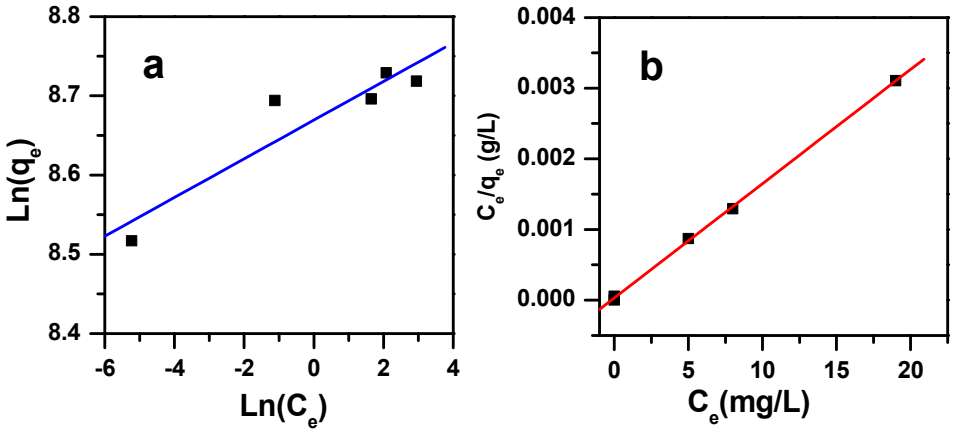

Figure 9. Plots of (**a**) the Freundlich and (**b**) Langmuir isotherms displaying the initial dye concentration effect on the removal of MB by $Fe_2(MoO_4)_3$.

Table 5. MB removal by $Fe_2(MoO_4)_3$ isotherm parameters.

Langmuir				Freundlich			Temkin			Dubinin-Radushkevich		
q_m (mg/g)	K_L (L/mg)	R^2	Range R_L	q_F ($mg^{(1-1/n)}L^{1/n}g^{-1}$)	1/n	R^2	A_T (L/g)	B_T	R^2	q_m (mg/g)	R^2	E (Kj/mol)
6173	5	0.999	0.0024–0.0038	5825	0.02	0.866	5E18	135	0.870	6063	0.971	944

Table 6. The maximum removed amount (q_m) of MB dye reported in the literature.

Nanosorbent	q_m (mg/g)	Reference
Magnetic β-cyclodextrin-chitosan nanoparticles	2783.30	[55]
Fe_2O_3	1124.70	[56]
Zinc molybdate nanoparticles	217.86	[23]
CoO	5501.93	[56]
Molybdenum trioxide nanorods and stacked nanoplates	152.00	[45]
Iron molybdate ($Fe_2(MoO_4)_3$)	6173.00	This work

2.4. Regeneration and Characterization of the $Fe_2(MoO_4)_3$ Nanosorbent

2.4.1. Regeneration Efficiency

The repeatability and regeneration of the nanosorbent are very important parameters for its eventual practical applications. In the literature, several regeneration procedures were suggested, such as microwave irradiation, bio-regeneration, supercritical regeneration, chemical extraction, thermal treatment, etc. [17,45,57–59]. The thermal regeneration used in the present work was similar

to that discussed in our previous work [45]. In this research, this thermal treatment method was tested for the regeneration process, as the structure of the $Fe_2(MoO_4)_3$ removal agent was stable.

The results showed that $Fe_2(MoO_4)_3$ was prone to regeneration by thermal treatment.

Figure 10 shows the recycled efficiency of $Fe_2(MoO_4)_3$ for the removal of methylene blue for three cycles. In fact, the results showed a decrease of dye removal from 99% to 96%, with a decreasing removal capacity from 5932 to 5777 mg/g. The adsorbent regeneration through calcination at 400 °C under air atmosphere was shown to be extremely efficient, in addition to its excellent reusability, as suggested by the observed high removal efficiencies.

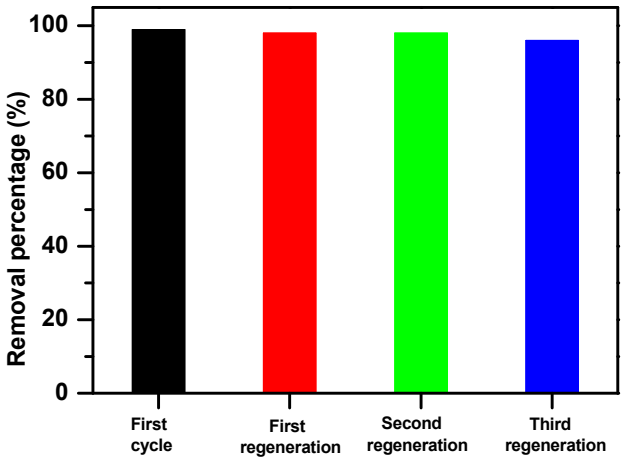

Figure 10. Recycled efficiencies of $Fe_2(MoO_4)_3$ for the removal of methylene blue (60 ppm, 0.001 g, 30 min).

2.4.2. Fourier-Transform Infrared Spectroscopy

With the aim of fully elucidating the removal process of MB dye by $Fe_2(MoO_4)_3$ nanosorbent, an FTIR spectroscopic study was carried out on the material prior to and after exposure to MB dye. Figure 11 displays the spectra of the $Fe_2(MoO_4)_3$ nanosorbent in both cases. As can be noticed, clear flexing and stretching vibrations characteristic of the metal-oxygen bonds were situated at frequencies between 700 and 1000 cm^{-1}, corresponding to the vibrations of the Mo–O bond of the MoO_4 tetrahedra in the $Fe_2(MoO_4)_3$ [60]. The pure MB spectrum exhibited bands between 1700 and 1000 cm^{-1} [61], while after MB adsorption, additional bands located at 1600 cm^{-1} were shown in the FTIR spectrum of ($Fe_2(MoO_4)_3$–MB). These were attributed to MB C=C bond stretching, inferring the presence of MB as a result of its attachment to $Fe_2(MoO_4)_3$-active sites [62]. The regenerated $Fe_2(MoO_4)_3$ FTIR spectrum, hereby denoted as ($Fe_2(MoO_4)_3$–MB-Reg), obtained upon thermal treatment was very much comparable with that of fresh $Fe_2(MoO_4)_3$, indicating the complete combustion of the attached MB on the surface. In addition, the obtained spectrum confirmed the purity of the regenerated material and the efficiency of the reused adsorbent. In the same sense, the X-ray diffraction (XRD) pattern of iron molybdate was taken before and after the regeneration, showing the same results.

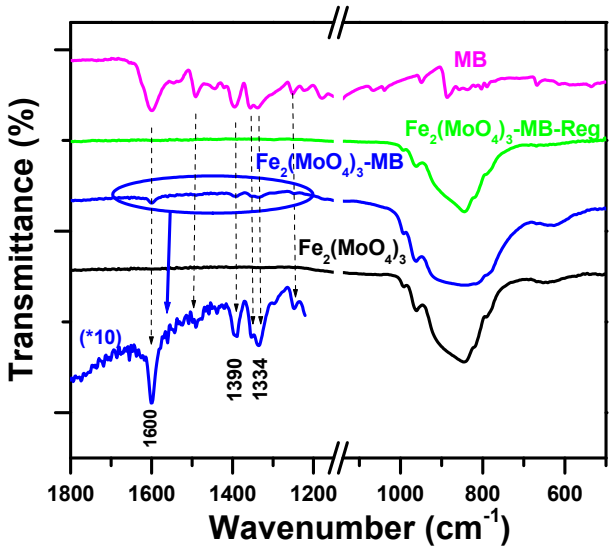

Figure 11. Fourier-transform infrared (FTIR) spectra of $Fe_2(MoO_4)_3$, $Fe_2(MoO_4)_3$–MB, $Fe_2(MoO_4)_3$–MB-Reg and MB.

2.5. MB Removal Mechanism

As discussed earlier, MB removal by $Fe_2(MoO_4)_3$ nanoparticles was found to proceed via an adsorption mechanism. In this respect, FTIR spectroscopic data depicted that no chemical decomposition of MB took place during its removal upon adsorption of the dye's cations, and there was no evidence of any intermediate compounds. Moreover, the removal effectiveness of MB using $Fe_2(MoO_4)_3$ nanoparticles increased with increasing pH values up to 11, which were attributed to the alkaline media. From these findings, we proposed the removal mechanism given in Figure 12. During the first step, MB (pKa = 3.8) maintained its positive charge at pH 11 [40]. In the same conditions, the iron molybdate ($Fe_2(MoO_5^{2-})_3$) ion was produced, without intermediate compounds, by the reaction of $Fe_2(MoO_4)_3$ with the hydroxyl groups (OH^-) present in solution [63]. Hence, the electrostatic interactions were governing the adsorptive process. These strong interactions were notable between the negatively charged iron molybdate ($Fe_2(MoO_5^{2-})_3$) surface and the positively charged MB cations [45].

To gain insights, at each adsorption step, into the morphological evolution of the $Fe_2(MoO_4)_3$ nanosorbent, SEM micrograph images were taken, as shown in Figure 13, which provided some indication of how the starting pure iron molybdate ($Fe_2(MoO_4)_3$) particles formed aggregates and showed good porosity, which could permit better adsorption of the dye (Figure 13A). However, the micrographs in Figure 13B,D,F,H indicated a less porous powder after the adsorption tests, i.e., the MB molecules filled the pores existing in the starting samples. Figure 13C,E,G,I showed that the sample morphology was not changed after regeneration and the first, second and third reuse. For all three cases, these less-agglomerated particles manifested as extremely porous powder. Generally, the morphology of $Fe_2(MoO_4)_3$ was not considerably altered, even after the second or third reuse, as shown in Figure 13G,I.

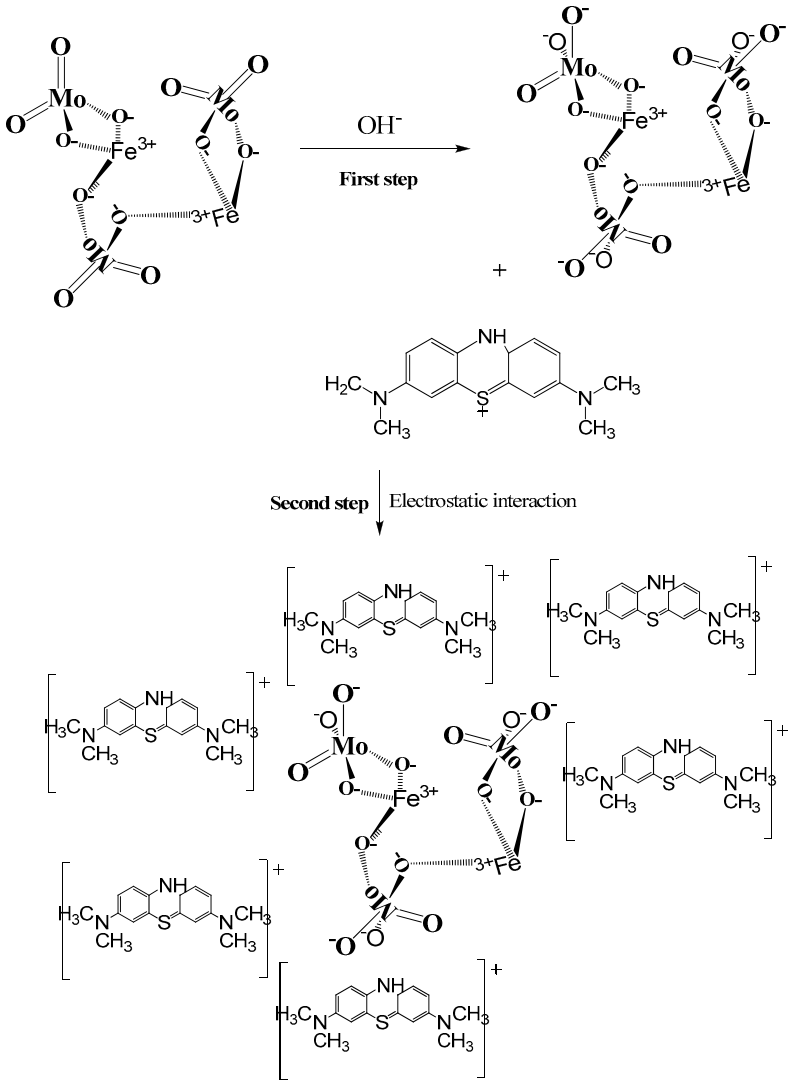

Figure 12. Schematic mechanism of MB dye removal using the iron molybdate nanosorbent.

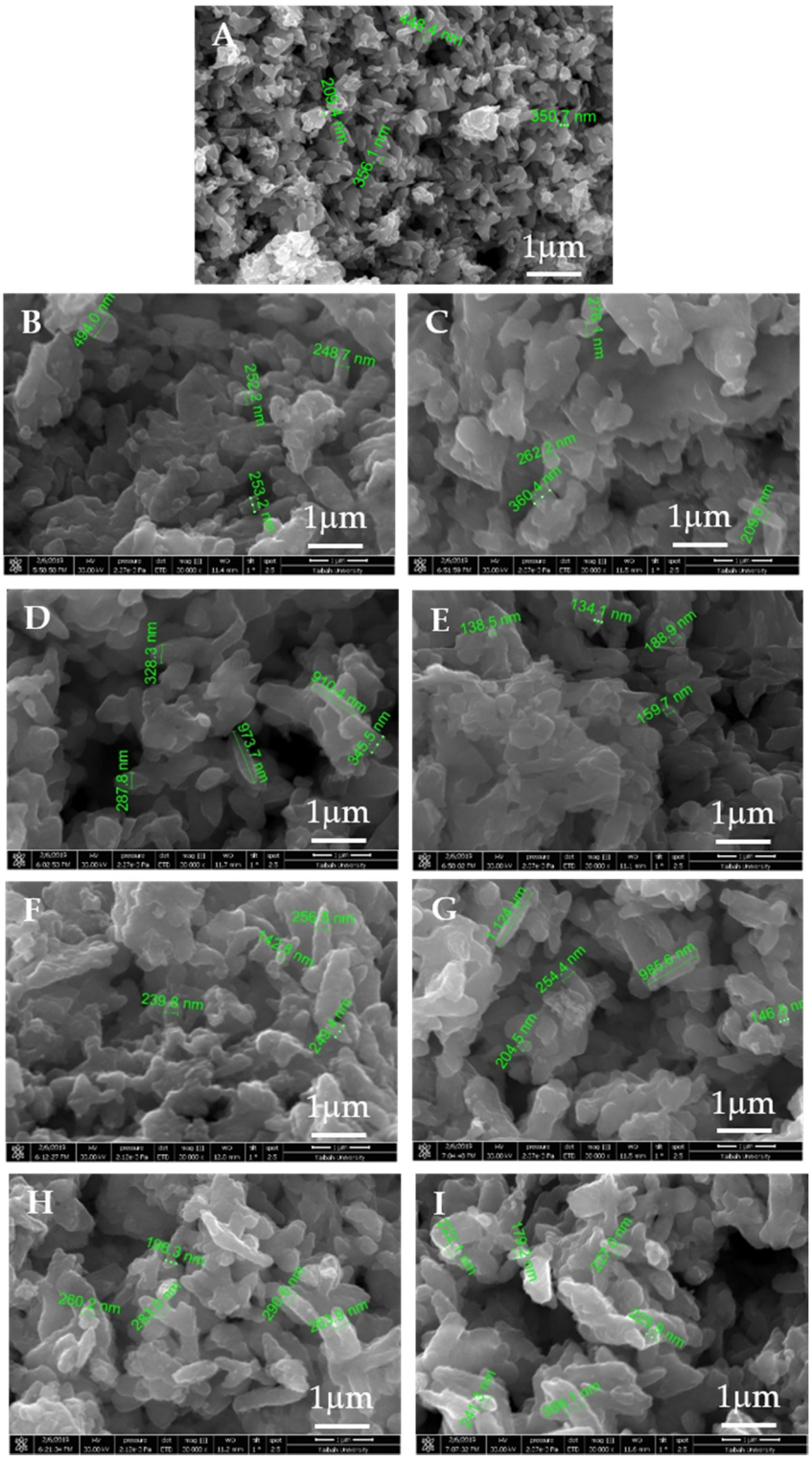

Figure 13. SEM micrographs of iron molybdate ($Fe_2(MoO_4)_3$): (**A**) the starting pure iron molybdate, (**B**) after MB dye removal, (**C**) after the first regeneration, (**D**) after the first removal cycle of MB dye, (**E**) after the second regeneration process, (**F**) after the second removal cycle of MB dye, (**G**) after the third regeneration process, (**H**) after the third removal cycle of MB dye and (**I**) the morphology of $Fe_2(MoO_4)_3$ after the final regeneration process.

3. Experimental

3.1. Iron Molybdate Nanosorbent Preparation

All chemicals were purchased from Sigma-Aldrich (St. Louis, MO, USA) and used as received without any changes, except for the methylene blue (MB) dye, which was supplied by Panreac, Barcelona, Spain.

Iron molybdate nanosorbent ($Fe_2(MoO_4)_3$) was produced by iron molybdenum complex thermal breakdown, in the solid state, by reacting iron nitrate ($Fe(NO_3)_3{\cdot}9H_2O$), oxalic acid ($H_2C_2O_4{\cdot}2H_2O$) and ammonium molybdate ($(NH_4)_6Mo_7O_{24}{\cdot}4H_2O$), as reported previously in the literature [22]. Iron nitrate ($Fe(NO_3)_3{\cdot}9H_2O$), oxalic acid ($H_2C_2O_4{\cdot}2H_2O$) and ammonium molybdate ($(NH_4)_6Mo_7O_{24}{\cdot}4H_2O$) were mixed together in a molar ratio of 2:10:0.43. The obtained homogeneously powdered mixture was heated at 160 °C on a hot plate. The iron molybdenum complex obtained was then decomposed in a tubular furnace (with both ends open) at 500 °C under static air for two hours.

3.2. Adsorption Investigations

Methylene blue (MB) dye removal was investigated in batch equilibrium experiments [38]. The MB solution pH was controlled by the addition of either 0.01-N HCl or 0.01-N NaOH solutions. The removal of MB by $Fe_2(MoO_4)_3$ was conducted with continual stirring of a specific quantity of the nanosorbent in MB solution (V = 100 mL) with known concentrations at various temperatures (T = 25 °C, 50 °C and 70 °C) and for different contact times (10 min, 30 min, 60 min, 90 min and 120 min). Next, a 0.22-µm (Whatman) syringe filter was employed to filter the solution, which was then investigated by UV-visible spectrometry at λ_{max} = 665 nm (Thermo Fisher Scientific, Madison, WI, USA). The percentage removed (%) and the amount of MB removed at equilibrium (q_e (mg/g)) were determined using the following equations:

$$\text{Removal } \% = \frac{C_0 - C_e}{C_0} \times 100 \tag{13}$$

$$q_e = \frac{(C_0 - C_e)}{M} \times V \tag{14}$$

where C_0 and C_e (ppm) are the initial and equilibrium concentrations of MB, respectively, M (g) is the added mass of $Fe_2(MoO_4)_3$ and V (L) is the volume of solution used. The results were reported in triplicate.

3.3. Method for Adsorbent Regeneration

For the experiments of adsorbent regeneration, an extended equilibrium time of 1 h was allocated for the removal with a 60-ppm solution that was used. The fresh $Fe_2(MoO_4)_3$ used was calcined for 1 h at 400 °C under atmospheric air after being dried at 100 °C upon filtration. The calcined $Fe_2(MoO_4)_3$ was tested for recycling purposes with the same conditions as that of freshly used $Fe_2(MoO_4)_3$. The whole regeneration cycle was repeated thrice under the same conditions. The removed percentage (%) and the MB dye amount removed at equilibrium (q_e (mg/g)) were determined using Equations (13) and (14).

3.4. Characterization

Analysis of XRD ($\lambda_{Cu\text{-}K\alpha}$ = 1.5406 Å and Ni filter on a Shimadzu X-ray diffractometer 6000, Tokyo, Japan) was carried out for the identification of the synthetized $Fe_2(MoO_4)_3$ nanosorbent material before and after its use for the removal of MB dye, as presented in Figure 14. The Scherrer equation was used to estimate the particle size from the XRD pattern of the as-prepared nanoparticles as follows: $D_{XRD} = 0.9\lambda/(\beta\cos\theta)$, where D_{XRD} is the average particle diameter, λ is the Cu kα wavelength, β is the full-width at half-maximum (FWHM) of the diffraction peak and θ is the diffraction angle. The first

two peaks were used to calculate the crystallite size D_{XRD}, and the crystallite size was found to be 45 nm in both cases.

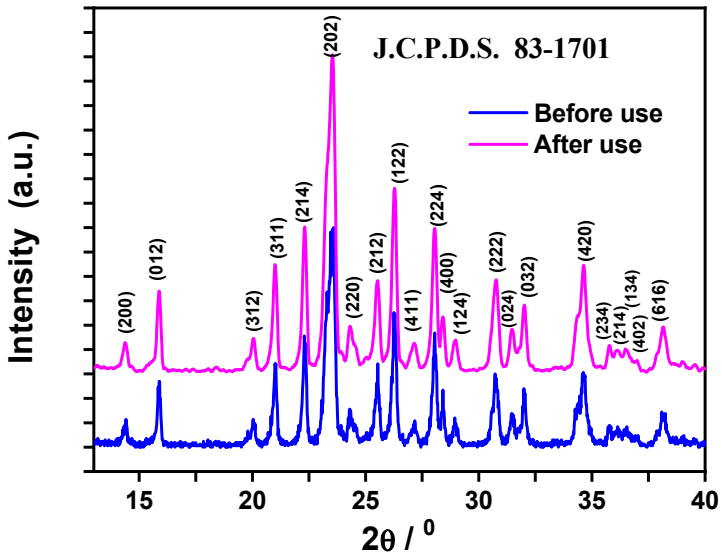

Figure 14. X-ray diffraction pattern of the synthetized $Fe_2(MoO_4)_3$ nanoparticle powder before and after its use for the removal of MB dye. The Joint Committee on Powder Diffraction Standards (J.C.P.D.S) index file is 83-1701.

The nitrogen adsorption isotherm was employed for the determination of the specific surface area [22] with a value close 8.03 m^2/g.

The presence of MB dye molecules on the $Fe_2(MoO_4)_3$ nanoparticles was confirmed by FTIR spectroscopy, using the KBr pellet technique in the range of 400 to 4000 cm^{-1}, on a Shimadzu apparatus (IR Affinity-1S, Shimadzu, Tokyo, Japan).

A Quanta FEG 250 scanning electron microscope (SEM; Thermo Fisher Scientific, Hillsboro, OR, USA) was used to study the surface morphology and the particle sizes of the synthesized materials.

The concentration at equilibrium of the MB dye was determined using a UV-visible spectrophotometer (Thermo Scientific Genesys 10S, Madison, WI, USA).

4. Conclusions

$Fe_2(MoO_4)_3$ nanosorbent was synthesized and utilized as an MB removal agent in aqueous solutions. A strongly pH-dependent removal was observed, with an achieved removal efficiency of 99% after only 120 min of contact time at pH 11, using an initial dye concentration of 50 to 60 ppm. Further kinetic investigations revealed that MB removal followed a pseudo-second-order model, while the thermodynamic study showed that the Langmuir isotherm was the best fitted model to the experimental adsorption data. Interestingly, Langmuir model-based calculations showed that the removal capacity attained a maximum of 6173 mg/g. Efficient regeneration was possible upon calcination at 400 °C, and afterwards, the nanosorbent was ready for further reuse. The $Fe_2(MoO_4)_3$ removal efficiency for MB was higher even after three cycles of reuse. The data showed that $Fe_2(MoO_4)_3$ was indeed as an effective nanosorbent, endowed with excellent removal performance for the studied MB dye, and that it was not altered after several recycling tests.

Author Contributions: Conceptualization, S.R., H.O.H. and A.M.; Methodology, A.M., S.R., and H.O.H.; Validation, S.R., H.O.H., F.K., M.A., and A.M.; Formal Analysis, H.O.H., A.M., S.R., M.A., F.K., and S.B.A.; Investigation, S.R., H.O.H., A.M., F.K., and M.A.; Resources, H.O.H., M.A., A.M., and F.K., S.R.; Data Curation, H.O.H., A.M., M.A. and F.K.; Writing-Original Draft Preparation, S.R., H.O.H. and A.M.; Writing-Review & Editing, S.B.A., F.K., M.A., and H.O.H.; Visualization, S.R., H.O.H., A.M., F.K., M.A., and S.B.A.; Supervision, S.R., and H.O.H.; Project Administration, S.R., and H.O.H.; Funding Acquisition, A.M., S.R., H.O.H., F.K., and M.A. All authors have read and agreed to the published version of the manuscript.

Funding: This research received no external funding.

Conflicts of Interest: The authors declare no conflict of interest.

References

1. Sakamoto, M.; Tofayel, A.; Begum, S.; Huq, H. Water Pollution and the Textile Industry in Bangladesh: Flawed Corporate Practices or Restrictive Opportunities? *Sustainability* **2019**, *11*, 1951. [CrossRef]
2. Ulson de Souza, S.M.A.G.; Forgiarini, E.; Ulson de Souza, A.A. Toxicity of textile dyes and their degradation by the enzyme horseradish peroxidase (HRP). *J. Hazard Mater.* **2007**, *147*, 1073–1078. [CrossRef] [PubMed]
3. Wu, M.; Yu, W.; Qu, J.; Gregory, J. The variation of flocs activity during floc breakage and aging, adsorbing phosphate, humic acid and clay particles. *Water Res.* **2019**, *155*, 131–141. [CrossRef] [PubMed]
4. Greluk, M.; Hubicki, Z. Effect of basicity of anion exchangers and number and positions of sulfonic groups of acid dyes on dyes adsorption on macroporous anion exchangers with styrenic polymer matrix. *Chem. Eng. J.* **2013**, *215–216*, 731–739. [CrossRef]
5. Piai, L.; Blokland, M.; van der Wal, A.; Langenhoff, A. Biodegradation and adsorption of micropollutants by biological activated carbon from a drinking water production plant. *J. Hazard. Mater.* **2020**, *388*, 122028. [CrossRef]
6. Cornelia, P.; Oana, P.; Robert, I.; Simona, G.M. Effective removal of methylene blue from aqueous solution using a new magnetic iron oxide nanosorbent prepared by combustion synthesis. *Clean Technol. Environ. Policy* **2016**, *18*, 705–715.
7. Liu, T.; Zhou, H.; Graham, N.; Yu, W.; Sun, K. 2D kaolin ultrafiltration membrane with ultrahigh flux for water purification. *Water Res.* **2019**, *156*, 425–433. [CrossRef] [PubMed]
8. Forgacs, E.; Cserhati, T.; Oros, G. Removal of synthetic dyes from wastewaters: A review. *Environ. Int.* **2004**, *30*, 953–971. [CrossRef] [PubMed]
9. Jiang, R.; Lu, G.; Yan, Z.; Wu, D.; Zhou, R.; Bao, X. Insights into a CQD-$SnNb_2O_6$/BiOCl Z-scheme system for the degradation of benzocaine: Influence factors, intermediate toxicity and photocatalytic mechanism. *Chem. Eng. J.* **2019**, *374*, 79–90. [CrossRef]
10. Miyah, Y.; Lahrichi, A.; Idrissi, M.; Khalil, A.; Zerrouq, F. Adsorption of methylene blue dye from aqueous solutions onto walnut shells powder: Equilibrium and kinetic studies. *Surf. Interface* **2018**, *11*, 74–81. [CrossRef]
11. Kang, S.; Zhao, Y.; Wang, W.; Zhang, T.; Chen, T.; Yi, H.; Rao, F.; Song, S. Removal of methylene blue from water with montmorillonite nanosheets/chitosan hydrogels as adsorbent. *Appl. Surf. Sci.* **2018**, *448*, 203–211. [CrossRef]
12. Chen, Y.H. Synthesis, characterization and dye adsorption of ilmenite nanoparticles. *J. Non-Cryst. Solids* **2011**, *357*, 136–139. [CrossRef]
13. Ozdemir, U.; Ozbay, I.; Ozbay, B.; Veli, S. Application of economical models for dye removal from aqueous solutions: Cash flow, cost–benefit and alternative selection methods. *Clean Technol. Environ. Policy* **2014**, *16*, 423–429. [CrossRef]
14. Chen, X.; Liu, L.; Luo, Z.; Shen, J.; Ni, Q.; Yao, J. Facile preparation of a cellulose-based bioadsorbent modified by hPEI in heterogeneous system for high-efficiency removal of multiple types of dyes. *React. Funct. Polym.* **2018**, *125*, 77–83. [CrossRef]
15. Rezk, M.Y.; Zeitoun, M.; El-Shazly, A.N.; Omar, M.M.; Allam, N.K. Robust photoactive nanoadsorbents with antibacterial activity for the removal of dyes. *J. Hazard. Mater.* **2019**, *378*, 120679. [CrossRef] [PubMed]
16. Low, S.K.; Tan, M.C. Dye adsorption characteristic of ultrasound pre-treated pomelo peel. *J. Environ. Chem. Eng.* **2018**, *6*, 3502–3509. [CrossRef]

17. Rakass, S.; Mohmoud, A.; Oudghiri-Hassani, H.; Abboudi, M.; Kooli, F.; Al Wadaani, F. Modified Nigella Sativa Seeds as a Novel Efficient Natural Adsorbent for Removal of Methylene Blue Dye. *Molecules* **2018**, *23*, 1950. [CrossRef]
18. Kittappa, S.; Jais, F.M.; Ramalingam, M.; Ibrahim, S. Functionalized magnetic mesoporous palm shell activated carbon for enhanced removal of azo dyes. *J. Environ. Chem. Eng.* **2020**, *8*, 104081. [CrossRef]
19. Widiyastuti, W.; Rois, M.F.; Suari, N.M.I.P.; Setyawan, H. Activated carbon nanofibers derived from coconut shell charcoal for dye removal application. *Adv. Powder Technol.* **2020**, *31*, 3267–3273. [CrossRef]
20. Madrakian, T.; Afkhami, A.; Ahmadi, M.; Bagheri, H. Removal of some cationic dyes from aqueous solutions using magnetic modified multi-walled carbon nanotubes. *J. Hazard Mater.* **2011**, *196*, 109–114. [CrossRef]
21. Oyewo, O.A.; Elemike, E.E.; Onwudiwe, D.C.; Onyango, M.S. Metal oxide-cellulose nanocomposites for the removal of toxic metals and dyes from wastewater. *Int. J. Biol. Macromol.* **2020**, *164*, 2477–2496. [CrossRef]
22. Oudghiri-Hassani, H. Synthesis, characterization and catalytic performance of iron molybdate $Fe_2(MoO_4)_3$ nanoparticles. *Catal. Commun.* **2015**, *60*, 19–22. [CrossRef]
23. Oudghiri-Hassani, H.; Rakass, S.; Abboudi, M.; Mohmoud, A.; Al Wadaani, F. Preparation and Characterization of α-Zinc Molybdate Catalyst: Efficient Sorbent for Methylene Blue and Reduction of 3-Nitrophenol. *Molecules* **2018**, *23*, 1462. [CrossRef] [PubMed]
24. Al-Wadaani, F.; Omer, A.; Abboudi, M.; Oudghiri-Hassani, H.; Rakass, S.; Messali, M.; Benaissa, M. High Catalytic Efficiency of Nanostructured β-$CoMoO_4$ in the Reduction of the *Ortho-*, *Meta-* and *Para*-Nitrophenol Isomers. *Molecules* **2018**, *23*, 364. [CrossRef] [PubMed]
25. Oudghiri-Hassani, H.; Al Wadaani, F.T. Preparation, Characterization and Catalytic Activity of Nickel Molybdate ($NiMoO_4$) Nanoparticles. *Molecules* **2018**, *23*, 273. [CrossRef]
26. Karaoglu, E.; Baykal, A. $CoFe_2O_4$–Pd (0) Nanocomposite: Magnetically Recyclable Catalyst. *J. Supercond Nov. Magn.* **2014**, *27*, 2041–2047. [CrossRef]
27. Wang, L.; Wang, H.; Wang, A.; Liu, M. Surface Modification of a Magnetic SiO_2 Support and Immobilization of a Nano-TiO_2 Photocatalyst on It. *Chinese J. Catal.* **2009**, *30*, 939–944. [CrossRef]
28. Ferreira, E.A.C.; Andrade Neto, N.F.; Bomio, M.R.D.; Motta, F.V. Influence of solution pH on forming silver molybdates obtained by sonochemical method and its application for methylene blue degradation. *Cer. Inter.* **2019**, *45*, 11448–11456. [CrossRef]
29. Oudghiri Hassani, H. Synthesis, Characterization and Application of Chromium Molybdate for Oxidation of Methylene Blue Dye. *J. Mater. Environ. Sci.* **2018**, *9*, 1051–1057.
30. Jouali, A.; Salhi, A.; Aguedach, A.; Aarfane, A.; Ghazzaf, H.; Lhadi, E.K.; El krati, M.; Tahiri, S. Photo-catalytic degradation of methylene blue and reactive blue 21 dyes in dynamic mode using TiO_2 particles immobilized on cellulosic fibers. *J. Photochem. Photobio. A: Chem.* **2019**, *383*, 112013. [CrossRef]
31. Soares, A.P.V.; Portela, M.F.; Kiennemann, A. Methanol selective oxidation to formaldehyde over iron-molybdate catalysts. *Catal. Rev.* **2004**, *47*, 125–174. [CrossRef]
32. Kersen, U.; Holappa, L. Surface characterization and H_2S-sensing potential of iron molybdate particles produced by supercritical solvothermal method and subsequent oxidation. *Appl. Phys. A Mater. Sci. Process.* **2006**, *85*, 431–436. [CrossRef]
33. Carlsson, P.-A.; Jing, D.; Skoglundh, M. Controlling Selectivity in Direct Conversion of Methane into Formaldehyde/Methanol over Iron Molybdate via Periodic Operation Conditions. *Energy Fuel* **2012**, *26*, 1984–1987. [CrossRef]
34. Ivanov, I.K.; Yankov, D.D. Deactivation of an industrial iron-molybdate catalyst for methanol oxidation. *Catal. Today* **2010**, *154*, 250–255. [CrossRef]
35. Kong, L.; Zhang, M.; Liu, X.; Ma, F.; Wei, B.; Wumaier, K.; Zhao, J.; Lu, Z.; Sun, J.; Chen, J.; et al. Green and rapid synthesis of iron molybdate catalyst by mechanochemistry and their catalytic performance for the oxidation of methanol to formaldehyde. *Chem. Eng. J.* **2019**, *364*, 390–400. [CrossRef]
36. Wang, L.; Huang, X.; Han, M.; Lyu, L.; Li, T.; Gao, Y.; Zeng, Q.; Hu, C. Efficient inhibition of photogenerated electron-hole recombination through persulfate activation and dual-pathway degradation of micropollutants over iron molybdate. *Appl. Catal. B Environ.* **2019**, *257*, 117904. [CrossRef]
37. Rashad, M.M.; Ibrahim, A.A.; Rayan, D.A.; Sanad, M.M.S.; Helmy, I.M. Photo-Fenton-like degradation of Rhodamine B dye from waste water using iron molybdate catalyst under visible light irradiation. *Environ. Nanotechnol. Monit. Manag.* **2017**, *8*, 175–186. [CrossRef]

38. Ganguly, P.; Sarkhel, R.; Das, P. Synthesis of pyrolyzed biochar and its application for dye removal: Batch, kinetic and Isotherm with linear and non-linear mathematical analysis. *Surf. Inter.* **2020**, *20*, 100616. [CrossRef]
39. Alver, E.; Metin, A.U. Anionic dye removal from aqueous solutions using modified zeolite: Adsorption kinetics and isotherm studies. *Chem. Eng. J.* **2012**, *200*, 59–67. [CrossRef]
40. Jihyun, R.K.; Santiano, B.; Kim, H.; Kan, E. Heterogeneous Oxidation of Methylene Blue with Surface-Modified Iron-Amended Activated Carbon. *Am. J. Anal. Chem.* **2013**, *4*, 115–122.
41. Kooli, F.; Liu, Y.; Abboudi, M.; Oudghiri Hassani, H.; Rakass, S.; Ibrahim, S.M.; Al-Wadaani, F. Waste bricks applied as removal agent of Basic Blue 41 from aqueous solution: Base treatment and their regeneration efficiency. *Appl. Sci.* **2019**, *9*, 1237. [CrossRef]
42. Kooli, F.; Liu, Y.; Hbaieb, K.; Ching, O.Y.; Al-Faze, R. Characterization of organo-kenyaites: Thermal stability and their effects on eosin removal characteristics. *Clay Miner.* **2018**, *53*, 91–104. [CrossRef]
43. Annan, N.; Karuppasamy, K. Low cost adsorbents for the removal of phenyl acetic acid from aqueous solution. *Indian J. Environ. Protec.* **1998**, *18*, 683–690.
44. Mahmoud, D.K.; Salleh, M.A.M.; Karim, W.A.W.A.; Idris, A.; Abidin, Z.Z. Batch adsorption of basic dye using acid treated kenaf fibre char: Equilibrium, kinetic and thermodynamic studies. *Chem. Eng. J.* **2012**, *181–182*, 449–457. [CrossRef]
45. Rakass, S.; Oudghiri-Hassani, H.; Abboudi, M.; Kooli, F.; Mohmoud, A.; Aljuhani, A.; Al Wadaani, F. Molybdenum Trioxide: Efficient Nanosorbent for Removal of Methylene Blue Dye from Aqueous Solutions. *Molecules* **2018**, *23*, 2295. [CrossRef] [PubMed]
46. Krishnan, K.; Anirudhan, T.S. A Preliminary examination of the adsorption characteristics of Pb(II) ions using sulphurised activated carbon prepared from bagasse pith. *Indian J. Chem. Technol.* **2002**, *9*, 32–40.
47. Sahu, S.; Pahi, S.; Tripathy, S.; Singh, S.K.; Behera, A.; Sahu, U.K.; Patel, R.K. Adsorption of methylene blue on chemically modified lychee seed biochar: Dynamic, equilibrium, and thermodynamic study. *J. Mol. Liq.* **2020**, *315*, 113743. [CrossRef]
48. Patil, S.; Renukdas, S.; Patel, N. Removal of methylene blue, a basic dye from aqueous solutions by adsorption using teak tree (Tectona grandis) bark powder. *Int. J. Environ. Sci.* **2011**, *1*, 711–726.
49. Vadivelan, V.; Kumar, K.V. Equilibrium, kinetics, mechanism, and process design for the sorption of methylene blue onto rice husk. *J. Colloid Interface Sci.* **2005**, *286*, 90–100. [CrossRef]
50. Wang, J.; Guo, X. Adsorption kinetic models: Physical meanings, applications, and solving methods. *J. Haz. Mater.* **2020**, *390*, 122156. [CrossRef]
51. Furusawa, T.; Smith, J.M. Intraparticle mass transport in slurries by dynamic adsorption studies. *AIChE J.* **1974**, *20*, 88–93. [CrossRef]
52. Ezzati, R. Derivation of Pseudo-First-Order, Pseudo-Second-Order and Modified Pseudo-First-Order rate equations from Langmuir and Freundlich isotherms for adsorption. *Chem. Eng. J.* **2020**, *392*, 123705. [CrossRef]
53. Hu, Q.; Zhang, Z. Application of Dubinin–Radushkevich isotherm model at the solid/solution interface: A theoretical analysis. *J. Mol. Liq.* **2019**, *277*, 646–648. [CrossRef]
54. Dada, A.O.; Olalekan, A.P.; Olatunya, A.M.; Dada, O. Langmuir, Freundlich, Temkin and Dubinin-Radushkevich Isotherms Studies of Equilibrium Sorption of Zn^{2+} Unto Phosphoric Acid Modified Rice Husk. *J. Appl. Chem.* **2012**, *3*, 38–45.
55. Fan, L.; Zhang, Y.; Luo, C.; Lu, F.; Qiu, H.; Sun, M. Synthesis and characterization of magnetic beta-cyclodextrin-chitosan nanoparticles as nano-adsorbents for removal of methyl blue. *Int. J. Biol Macromol.* **2012**, *50*, 444–450. [CrossRef]
56. Li, L.H.; Xiao, J.; Liu, P.; Yang, G.W. Super adsorption capability from amorphousization of metal oxide nanoparticles for dye removal. *Sci. Rep.* **2015**, *5*, 9028. [CrossRef] [PubMed]
57. Erfan Sadatshojaei, E.; Esmaeilzadeh, F.; Fathikaljahi, J.; Barzi, S.E.H.S.; Wood, D.A. Regeneration of the Midrex Reformer Catalysts Using Supercritical Carbon Dioxide. *Chem. Eng. J.* **2018**, *343*, 748–758. [CrossRef]
58. Yanlong Sun, Y.; Zhang, B.; Zheng, T.; Wang, P. Regeneration of activated carbon saturated with chloramphenicol by microwave and ultraviolet irradiation. *Chem. Eng. J.* **2017**, *320*, 264–270.
59. Maisa El Gamal, M.; Mousa, H.A.; El-Naas, M.H.; Zacharia, R.; Judd, S. Bio-regeneration of activated carbon: A comprehensive review. *Sep. Purif. Technol.* **2018**, *197*, 345–359. [CrossRef]

60. Kersen, Ü.; Keiski, R.L. Preliminary study on the selective oxidation of H_2S over $LaVO_4$ and $Fe_2(MoO_4)_3$ oxides, produced by a solvothermal method. *Catal. Commun.* **2009**, *10*, 1039–1042. [CrossRef]
61. Ahmed, F.; Dewani, R.; Pervez, M.K.; Mahboob, S.J.; Soomro, S.A. Non-destructive FT-IR analysis of mono azo dyes. *Bulg. Chem. Commun.* **2016**, *48*, 71–77.
62. Etman, A.S.; Abdelhamid, H.N.; Yuan, Y.; Wang, L.; Zou, X.; Sun, J. Facile Water-Based Strategy for Synthesizing MoO_{3-x} Nanosheets: Efficient Visible Light Photocatalysts for Dye Degradation. *ACS Omega* **2018**, *3*, 2201–2209. [CrossRef] [PubMed]
63. Aracena, A.; Sannino, A.; Jerez, O. Dissolution kinetics of molybdite in KOH media at different temperatures. *Trans. Nonferrous Met. Soc. China* **2018**, *28*, 177–185. [CrossRef]

Sample Availability: Samples of the compounds iron molybdate ($Fe_2(MoO_4)_3$ are available from the authors.